Journal of Food Engineering 404 (2026) 112777

Contents lists available at ScienceDirect

Journal of Food Engineering

journal homepage: www.elsevier.com/locate/jfoodeng

Non-invasive detection of internal foreign bodies in foods by using air-coupled ultrasound: case studies in beef burger patties and jelly plates

Gentil A. Collazos-Escobar [a], José M. Prats-Montalbán [b], Anabella S. Giacomozzi [a], José Benedito [a], Tomas E. Gómez Álvarez-Arenas [c], José V. García-Pérez [a,*]

[a] Grupo de Análisis y Simulación de Procesos Agroalimentarios (ASPA), Instituto Universitario de Ingeniería de Alimentos–FoodUPV, Universitat Politécnica de València, Camí de Vera s/n, Edificio 3F, 46022, Valencia, Spain
[b] Grupo de Ingeniería Estadística Multivariante (GIEM), Universitat Politécnica de València (UPV), Camí de Vera s/n, Edificio 7A, 46022, Valencia, Spain
[c] Institute for Physical and Information Technologies, CSIC, Serrano 144, E28006, Madrid, Spain

ARTICLE INFO

Keywords:
Foreign bodies
Non-invasive detection
Air-coupled ultrasound
Acoustic properties
Real-time quality monitoring
Industrial inline inspection

ABSTRACT

The detection of foreign bodies in the food industry is of increasingly critical importance due to potential health hazards to consumers, adverse effects on company's reputation, and legal compliance concerns. Therefore, this work aimed to assess the feasibility of using air-coupled ultrasound to detect foreign bodies within beef burgers patties and jelly plates as heterogenous-solid and homogeneous-semi solid model foods. Different types of foreign bodies (metal and plastic) at two different sizes (10 and 5 mm) were embedded within the burger patties and jelly plates. Both Control and Out-of-Control (OC, with foreign bodies) samples were scanned using an automated 2D system and a pair of unfocused air-coupled ultrasound sensors (0.28 MHz) operating in through-transmission mode. From time-domain ultrasound signals, two energy-related ultrasound parameters (square norm and integral) were computed to create the ultrasonic images. The presence of foreign bodies within the food samples led to the attenuation of the ultrasound waves (avg. square norm and integral decrease from 94.4 to 41.0 %, depending on the food product and foreign body size and material). This enabled the mapping of defective areas in both square norm and integral ultrasonic C-Scan images. Histogram-based image analysis proved to be effective in distinguishing between control and OC samples, while also facilitating the establishment of a detection threshold for foreign body identification. The manuscript also illustrates how the use of unfocused air-coupled ultrasonic transducers may be extrapolated for industrial purposes by minimizing the number of array elements necessary to scan the whole product. The methodology proposed in this study offers significant promise for the reliable, rapid, and accurate detection of foreign bodies in solid and semi-solid food matrices, with great potential for further industrial implementation.

1. Introduction

Foreign body (FB) detection is essential for ensuring food safety and maintaining quality standards in the food industry. The presence of FBs in food products implies physical contamination and involves serious health risks to consumers (Zhao et al., 2006). Additionally, it can harm companys' reputation, compromise legal compliance and lead to costly recalls incidents (Edwards and Stringer, 2007). FBs encompass a wide range of materials, including metals, glass, plastic, insects, stones, or other unwanted substances that may inadvertently enter food products during processing, packaging or handling (Mohd Khairi et al., 2018). Substances inherent to the food itself, such as bone fragments in meat products or gas bubbles resulting from abnormal cheese fermentation, are also considered as FBs due to their association with deficient processing (Djekic et al., 2017).

The detection of FBs located on the food's surface does not represent a scientific challenge as these FBs can be readily detected using automated imaging techniques coupled to machine learning tools, which are already widely used for assessing product's properties, such as color or shape. However, the detection of internal FBs remains an important area of research despite the industrial application of techniques like magnetic detectors for ferrous metals and X-ray systems for identifying materials denser than the food matrix. In particular, the detection of the so-called "soft" contaminants, such as plastics, wood or insects cannot be

* Corresponding author.
E-mail address: jogarpe4@tal.upv.es (J.V. García-Pérez).

https://doi.org/10.1016/j.jfoodeng.2025.112777
Received 29 April 2025; Received in revised form 28 July 2025; Accepted 11 August 2025
Available online 12 August 2025

effectively achieved by aforementioned techniques. This represents one of the major challenges for quality control and safety in the food industry (Li et al., 2015). Thereby, alternative technologies for the detection of FBs in foods are actively being sought by the scientific community. Non-invasive photonic technologies, including near infrared spectroscopy, dielectric and hyperspectral imaging have been tested (Yaqoob et al., 2021), but its implementation seems to be constrained due to high costs, complexity, limited penetration depth, or reduced sensitivity to low-density FBs (Chen et al., 2013).

Ultrasound has proven to be a promising technology for automated, rapid, accurate, cost-effective and simple food quality inspection (Chandrapala, 2015). As a sound wave penetrates a food product and interacts with a FB, both its velocity and amplitude may be altered (Awad et al., 2012). These alterations primarily depend on FB's size and properties as well as the impedance mismatch between the FB and the surrounding material. Conventional contact ultrasound has been studied as a non-destructive technology for FBs detection (Mohd Khairi et al., 2015). Applications include the detection of bone fragments in deboned chicken breast (Correia et al., 2008), bone, glass, steel, and wood pieces within marmalade and cheese products (Hæggström and Luukkala, 2001), internal failures in cheese (Leemans and Destain, 2009), glass fragments in bottled beverages (Zhao et al., 2004), and stones and aluminum plates in canned foods (Meftah and Azimin, 2012). However, this contact-based approach requires the contact between the product and the sensor, often involving the use of coupling materials (water, oil, glycerin or gel) that can lead to surface contamination or even product damage. Additionally, the contact involves low measurement speeds due to the need to ensure effective and repetitive coupling of the ultrasonic transducer to the product (Chimenti, 2014). For these reasons, conventional contact ultrasound is regarded as a non-destructive but minimally invasive technology, which limits its feasibility for real-time industrial inspection.

In recent years, air-coupled ultrasound has emerged as a novel technique for replacing conventional contact methods (Fariñas et al., 2023), offering robustness in industrial settings, high sensitivity, fast testing rates and cost-effectiveness. This technology provides a non-destructive and non-invasive solution for on-line monitoring of all food products within each batch (Fariñas et al., 2023). Previous studies have explored air-coupled ultrasound for detecting FBs, but existing applications face limitations related to the type of ultrasonic transducers employed, which restrict their broader industrial use. Specific challenges include the low efficiency of high-frequency air-coupled transducers, which suffer from instability in air (Cho and Irudayaraj, 2003), the need for complex preprocessing in capacitive transducers (Gan et al., 2006; Pallav et al., 2009), and the requirement for electrically conductive samples when using electromagnetic acoustic transducers (Ho et al., 2007). These challenges have hindered the development of effective air-coupled ultrasound solutions for FB detection in recent years.

For an effective and robust industrial application of air-coupled ultrasound, it is essential that ultrasound sensors achieve a high Signal-to-Noise Ratio (SNR) and stable performance, minimizing disturbances from airflow and environmental conditions, such as temperature and relative humidity. Addressing the limitations of current ultrasound sensors is critical to achieving these objectives.

In this context, the use of piezoelectric transducers with tuned impedance matching layers (Gómez Álvarez-Arenas, 2004) provides a high SNR and an excellent air stability, enabling effective inspections in industrial environments. The effectiveness of this type of transducers has been demonstrated for the accurate inspection of a wide range of food products, such as avocado (Fariñas et al., 2021a), pork burger (Fariñas et al., 2021b), raw and dried potato (Sanchez-Jimenez et al., 2023) and raw and salted beef (Fariñas et al., 2023). In these previous works, average food properties, such as texture or composition, were estimated using air-coupled ultrasound by averaging measurements taken at multiple points. However, detecting FBs presents more challenging and different requirements, as the entire product must be scanned making it necessary to create and analyze an ultrasonic image of the scanned product (C-scan image). Thus, the aim of this study is to assess the feasibility of using an air-coupled ultrasound system, comprising tuned multilayer piezoelectric unfocused transducers, for rapid and non-invasive detection of FBs in food products. Commercial burgers patties and jelly plates will be examined as models for heterogenous solid and homogeneous semi-solid foods, respectively.

2. Materials and methods

2.1. Food samples and foreign bodies

Beef meat burgers (Fig. 1B, 90 g per patty, Elaborados Cárnicos Medina, Spain) were purchased from a local grocery store. The commercial samples selected for laboratory analysis consisted of beef (88 %), water, vegetable fiber (containing pea), cereal (rice), salt, flavouring, preservative (E−221) (sulphite), antioxidants (E−301 and E−331), and colouring agent (E−120), as provided by the manufacturer on the product label, which resulted in an average composition (g/100 g) of fat 14, carbohydrates 2.9, proteins 17 and salt 17. Patties were homogenized manually forming a ball and inserting the FB into its geometrical center. Afterwards, the burger patties were re-shaped again using an adjustable houseware mold (model AHM485, American Metalcraft, Inc., USA) consisting of two parallel stainless-steel circular plates to obtain the Out-of-Control (OC) samples (95 ± 2 mm diameter, 9.9 ± 0.1 mm thickness) (Fig. 1D). The same re-shaping procedure was applied to the Control burger samples to avoid differences on the patty structure (Fig. 1C). Finally, the re-shaped samples were stored at 4 °C for 24 h before ultrasonic inspection. The insertion of FBs into the geometrical center was complex since during the reshaping, the FB could shift away from the center.

As for the jellies, they were formulated as illustrated in Fig. 1. Firstly, a 5 % w/v bovine gelatin (CAS9000-70-8, Sigma-Aldrich, USA) solution was prepared using a magnetic stirrer coupled with a hotplate (Stuart-Scientific, UK) at 70 °C and 500 rpm for 10 min. The solution was then cooled to 50 °C (under room conditions of 27 ± 1 °C and 63 ± 6 %RH), and approximately 70 ± 1 g of the product was placed in polystyrene plates (86.4 ± 0.1 mm diameter, 12.5 ± 0.1 mm thickness) and covered with their corresponding polystyrene lids (Fig. 1A). Thereby, jelly plates are considered a packaged material model, which also represents a challenge for the ultrasonic analysis, due to the increase in the number of interfaces, leading to higher energy loss. For the OC jelly plates, the same procedure was followed and the FB was inserted into the center of the plate (Fig. 1E) before placing the lid.

As FBs, metal washer pieces (stainless steel 316) with external diameters of 5 and 10 mm (internal diameters of 2.7 and 3.3 mm, respectively and thickness of 1.6 mm) and soft plastic pieces (thermoplastic polyurethane) measuring 10 × 10 mm and 5 × 5 mm and thickness of 3.1 mm (Fig. 1) were used (Table 1). Both types of FBs are common materials in processing lines and may potentially contaminate food products due to equipment malfunctions or other incidents, representing a noticeable risk for the food quality and safety (Djekic et al., 2017). Three replicates were analyzed for each food product and type of FB. In addition, Control samples were also analyzed in triplicate. Thus, a total of 15 samples of burger patties and 15 samples of jellies were analyzed.

2.2. Characterization of food samples and FBs

Both food samples and FBs were characterized by measuring their density (ρ, kg/m^3) and ultrasonic velocity (v, m/s). Sample thickness (Th, mm) was measured using a digital caliper (192–633, Mitutoyo, Japan) and the sample area through a digital camera (Olympus E510, Olympus, USA) and the ImageJ software (Rasband, W.S., ImageJ v.1.43 s, National Institute of Health, Bethesda, Maryland, USA). For ρ and v characterization, food samples without FBs and larger metal and plastic

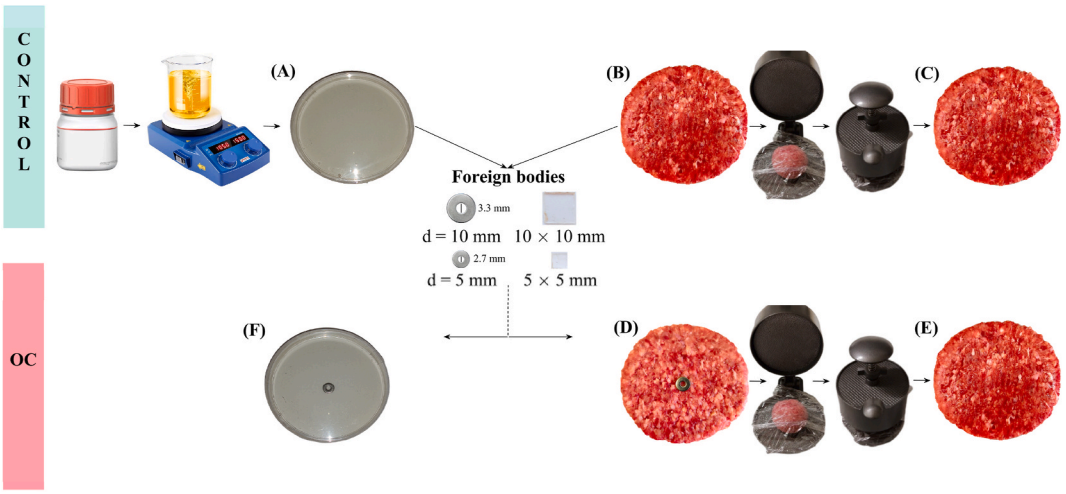

Fig. 1. Preparation of Control and Out-of-Control (OC) samples. Control (A) and OC (F) jellies, and Control (B and C) and OC (D and E) burger patties.

Table 1
Characterization of food samples and foreign bodies.

Parameter	Food samples		Foreign bodies	
	Burger patties	Jellies	Metal	Soft plastic
Th (mm)	9.90 ± 0.10	12.50 ± 0.10	1.60 ± 0.02	3.10 ± 0.01
ρ (kg/m^3)	1162.69 ± 5.77^a	1029.96 ± 8.20^b	7167.14 ± 4.53^c	1149.00 ± 4.56^a
v (m/s)	1507.50 ± 25.66^a	1329.83 ± 27.10^b	3155.25 ± 15.18^c	917.55 ± 16.42^d
Z (MRayl)	1.73 ± 0.05^a	1.37 ± 0.04^b	22.61 ± 0.09^c	1.05 ± 0.02^d

Th (thickness), ρ (density), TOF (Time-of-Flight), v (ultrasonic velocity), and Z (acoustic impedance). Mean ± standard error. Different lowercase letters indicate statistically significant differences (95 %) for each property.

pieces (50 × 50 mm) than those used in the OC samples preparation (section 2.1) were employed. Density was calculated by dividing the weight (PB3002-S, Mettler Toledo, USA) by the volume of samples (area × Th). v and acoustic specific impedance (Z, MRayl) were measured as detailed in section 2.4.

2.3. Experimental set-up for ultrasonic measurements

The experimental set-up used for ultrasonic measurements is illustrated in Fig. 2. The unfocused piezoelectric transducers operated in through-transmission mode, with a central frequency of 0.28 MHz, a peak sensitivity of −25 dB and active diameter of 27 mm (US-BioMat Lab., ITEFI-CSIC, Madrid, Spain). The transducers were perfectly aligned with each other and positioned 120 mm apart. The pulser-receiver

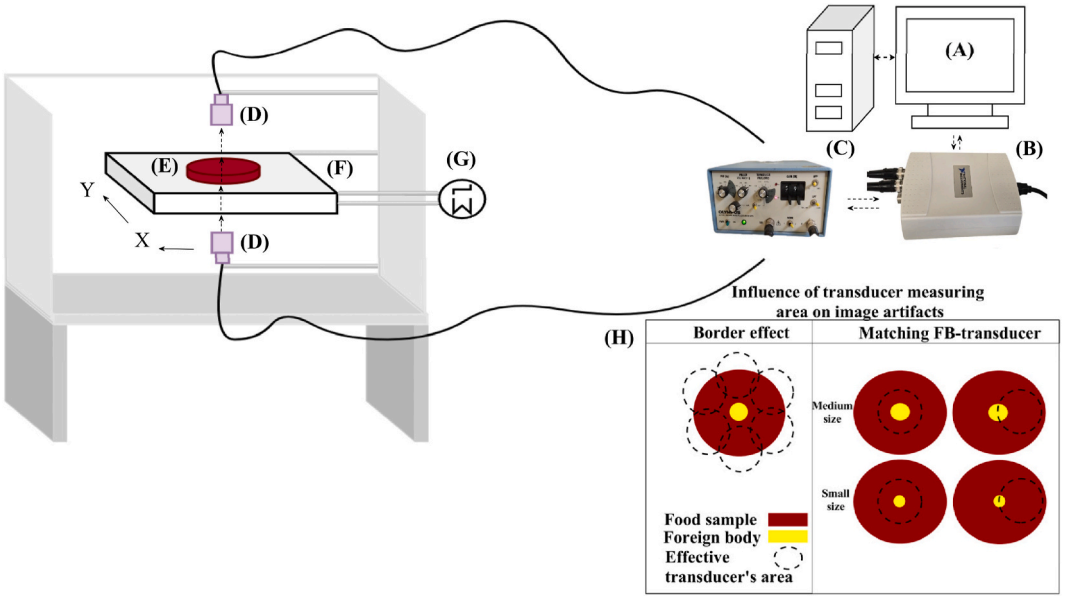

Fig. 2. Experimental set-up for ultrasonic image acquisition. Computer (A), digitizing card (B), pulser-receiver (C), piezoelectric air-coupled ultrasound transducers (D), food sample (E), holder (F), electrical stepper motors (G). Explanation of image artifacts (H).

instrument (Fig. 2C) (5077 PR, Olympus, Houston, TX, USA) emitted a semi-cycle square wave with an amplitude of 400 V fitted to the central frequency of the transducers (Fig. 2D). The signal of the receiver transducer was amplified by 59 dB, digitalized at 10 Mpoints s^{-1}, taking 7500 points, and averaged (n = 10) using a digital high-speed digitizer card (Fig. 2B) (NI 5133, National Instruments, Austin, TX, USA) linked through an USB connector to the PC (Fig. 2A). The synchronization output of the pulser was used as the trigger.

The food sample (Fig. 2E) was placed on a holder (Fig. 2F) consisting of a metal frame and a net made of fishing lines (0.2 mm) spaced 5 mm apart, with the purpose to provide mechanical support while minimizing interference with the ultrasonic beam.

The sample holder could be moved in the X and Y directions using an automated 2D positioning system consisting of two electrical stepper motors (Fig. 2G, Stepper Motor 4240-15A, Huizhou Bachin Electronic Technology Co, China) controlled by a CNC-based Arduino controller card (CNC Shield-GRBL, Huizhou Bachin Electronic Technology Co, China). All components of this system were managed through a software developed in LabVIEW® 2020 (National Instruments, Austin, TX, USA). Thereby, the ultrasound images (C-Scans) for both Control and OC food samples were generated by acquiring ultrasonic signals at 1 mm intervals in both X and Y directions across the surface of the food samples, using the automated 2D positioning system (Fig. 2). The scanned surface area was established considering the diameter of each sample (95 mm for burgers and 86.4 mm for jellies). As detailed in section 2.4, and to exclude the edge area in ultrasound images, a region of interest with smaller dimensions than the sample diameter was defined. Consequently, ultrasound images for burger patties measured 80 × 80 mm, producing 6400 signals, each with 7500 points, resulting in a total acquisition time per sample of approximately 6400 s (1.78 h), since each 2D movement in both X and Y directions across the product surface required 1 s. For jelly plates, the images measured 60 × 60 mm, yielding 3600 signals, each with 7500 points, corresponding to a total acquisition time per sample of approximately 3600 s (1 h). In this study, the acquisition time of the ultrasonic images was not optimized. However, the scanning process could be accelerated by minimizing the delay time between measurements and adjusting the number of averaged signals. The image acquisition process for the food samples was carried out under room conditions of 27 ± 1 °C and 63 ± 6 %RH.

2.4. Signal analysis and construction of ultrasonic images

Signal analysis involved determining energy-related parameters and the ultrasonic velocity (v) in the time domain. Specifically, the energy-related parameters square norm (SNORM, V^2) and the integral of signals (INT, μs), were computed in the time domain for both Control and OC signals and then, ultrasound images (C-Scans) of SNORM and INT were constructed. Signal analysis consisted of, firstly, a baseline correction to eliminate the offset (Garcia-Perez et al., 2019). Secondly, the energy related parameters, SNORM and INT, were calculated using Eq. (1) and Eq. (2), respectively.

$$\mathrm{SNORM} = \|A_s\|^2 \tag{1}$$

$$\mathrm{INT} = \mathrm{trapz}(A_s > 0) \tag{2}$$

where A_s represents the ultrasonic signal amplitude (V), which was calculated from 1800 to 7500 points and the "trapz" function in MATLAB® R2023a (The MathWorks Inc., Natick, MA, USA) was used to compute the area under the signal's curve using the trapezoidal numerical method. Both parameters were computed for each measuring point in the samples (pixel of the image).

Ultrasound images of Control and OC samples were obtained, encompassing spatial dimensions of 80 × 80 mm for burger patties and 60 × 60 mm for jellies. Each image was constructed from the individual ultrasonic signals acquired at each pixel position across the surface of the samples with a 2D spatial resolution of 1 mm. From each ultrasonic signal, the energy-related parameters SNORM and INT were computed, and these were used to generate two-channel ultrasound images (multichannel images) for each sample. The preprocessing of signals and images was performed using the MATLAB software.

Two important image artifacts linked to the interaction between the transducer's measuring area with both the food boundaries and the FB area need to be explained (Fig. 2H). When the sample is scanned near its boundaries, an edge effect appears if the food surface does not fully cover the transducer's effective measuring area. Consequently, part of the ultrasound energy travels through the air, which saturates the recorded signal and alters the energy-related ultrasonic parameters. For this reason, ultrasound images were acquired by scanning a smaller surface area than sample diameter (section 2.3), which does not disturb the results obtained in the present study since the FBs were located in the central zone of the food samples. Further works have to necessarily elucidate the feasibility of the ultrasonic technology to detect the FBs located near the sample edges. Another image artifact is related to the matching between the ultrasonic transducer's measurement area and the FB. The greatest impact of the FB on the ultrasonic wave is found when the transducer measurement area completely covers its surface; naturally, a larger FB area, results in a greater effect on the signal. However, the ultrasonic signal may be also altered in some extent when only a portion of the FB falls into the transducer measurement area (Fig. 2). This partial coverage may lead to blurred edges in the ultrasound images around the location of the FB.

In order to avoid the edge effect in the image analysis of Control and OC samples (as previously detailed), the air-coupled ultrasound images of SNORM and INT were processed, considering only the pixels of SNORM images lower than 90 V^2 and INT values below 180 V μs. Subsequently, both "histogram" and "histcounts" MATLAB function were used to compute the histogram and cumulative histograms of these images from Control and OC samples, respectively. To quantify the influence of FBs on both SNORM and INT images, the fist-order statistical parameter known as skewness (SKW) was computed using "skewness" MATLAB function from the histograms of these images. In addition, the cumulative histograms and their corresponding area under the curve (AUC) were also calculated. The AUC represents the integral of the cumulative histogram, providing a quantitative measure of the overall signal distribution within the sample.

In order to ultrasonically characterize the food samples and FBs, the Time-of-Flight (TOF) was assessed by the energy threshold method (ETM), as described by Garcia-Perez et al. (2019). Subsequently, to compute the v in the sample (Eq. (3)), the TOF change (ΔTOF) was considered as the difference between the reference signal (without sample, wave propagating between transducers through air) and the one propagated through the sample. Then the ultrasonic impedance (Z) of the samples was calculated from the product between v and density.

$$v = \frac{T_h}{\Delta TOF + \frac{T_h}{V_a}} \tag{3}$$

Where V_a corresponds to the velocity of sound in the air (346 m s^{-1} at 27 °C and 63 % RH).

Finally, to quantify the SNR of air-coupled ultrasound signals, the ratio between the signal amplitude to the noise amplitude was computed using Eq. (4). This calculation aimed to assess the SNR of our piezoelectric transducers to facilitate comparisons with other air-coupled ultrasound systems reported in the literature.

$$\mathrm{SNR} = \frac{\max(A_s) + |\min(A_s)|}{\max(A_{Snoise}) + |\min(A_{Snoise})|} \tag{4}$$

where A_{Snoise} represent the noise amplitude of the ultrasound signal calculated from 1300 to 1800 points.

In order to assess the potential industry application of air-coupled ultrasound technology, the ultrasonic images obtained for both

Control and OC served as the basis for simulating an industrial application of this technology. Therefore, from the ultrasound images of SNORM and INT, three different X-scans were extracted, namely, center scan (CSC), left scan (LSC), and right scan (RSC). CSC was captured from the center of the images, while LSC and RSC were captured by shifting 15 mm left and right, respectively. These three lines were then analyzed to determine the presence or absence of FBs, as will be detailed in the Results and Discussion section.

2.5. Statistical analysis

A one-way analysis of variance (ANOVA) was conducted to determine significant ($p < 0.05$) differences in ρ, v, and Z based on the type of food samples (burger patties and jelly plates) and foreign objects (section 2.4). Mean pairwise comparisons in the ANOVA model were performed using Fisher's Least Significant Difference (LSD) test, with a confidence level of 95 %.

A multifactor ANOVA was used to assess the influence of the type of food and the type of FB present in these foods on the energy-related ultrasound parameters (SNORM and INT, section 2.4). To this end, a 3 × 3 mm window was used to extract 9 pixels from the center of each SNORM and INT images of the three replicates. As a result, 27 pixels of SNORM and INT for Control and 27 pixels of SNORM and INT for each type (size and FB) of OC samples were used in the multifactor ANOVA model. To further elucidate the influence of the type of food and FB contained inside these samples on the SKW parameter derived from the SNORM and INT histograms, as well as on the AUC from the cumulative histograms of SNORM and INT, four multifactor ANOVA models were used, one for each response variable. Mean pairwise comparison of energy-related ultrasound parameters (SNORM and INT), the SKW and AUC parameters were performed using LSD intervals calculated at a 95 % confidence level. All ANOVA models underwent residual validation, which involved testing the residuals for normality (Shapiro-Wilk's test and q-q plot), independence (Ljung-Box's test), and homoscedasticity (Levene's test and multiple linear regression-MLR on square residuals) (Collazos-Escobar et al., 2023). Hypothesis tests and fulfillment of statistical assumptions were assessed at a 95 % confidence level. The statistical analysis was conducted using STATGRAPHICS Centurion XVIII (Manugistics, Inc., Rockville, MD, USA).

3. Results and discussion

3.1. Influence of foreign bodies on air-coupled ultrasound signals

The influence of FBs on air-coupled ultrasound signals obtained from Control and OC images of burger patties and jellies is illustrated in Fig. 3. Additionally, the characterization of food samples and FBs is presented in Table 1. For illustrative purposes, ultrasound signals from the center of Control and OC samples were randomly selected from the three replicates and are shown in Fig. 3. A similar behavior was observed in the remaining Control and OC signals. Fig. 3 shows how the presence of metal and plastic pieces of different sizes embedded within burger

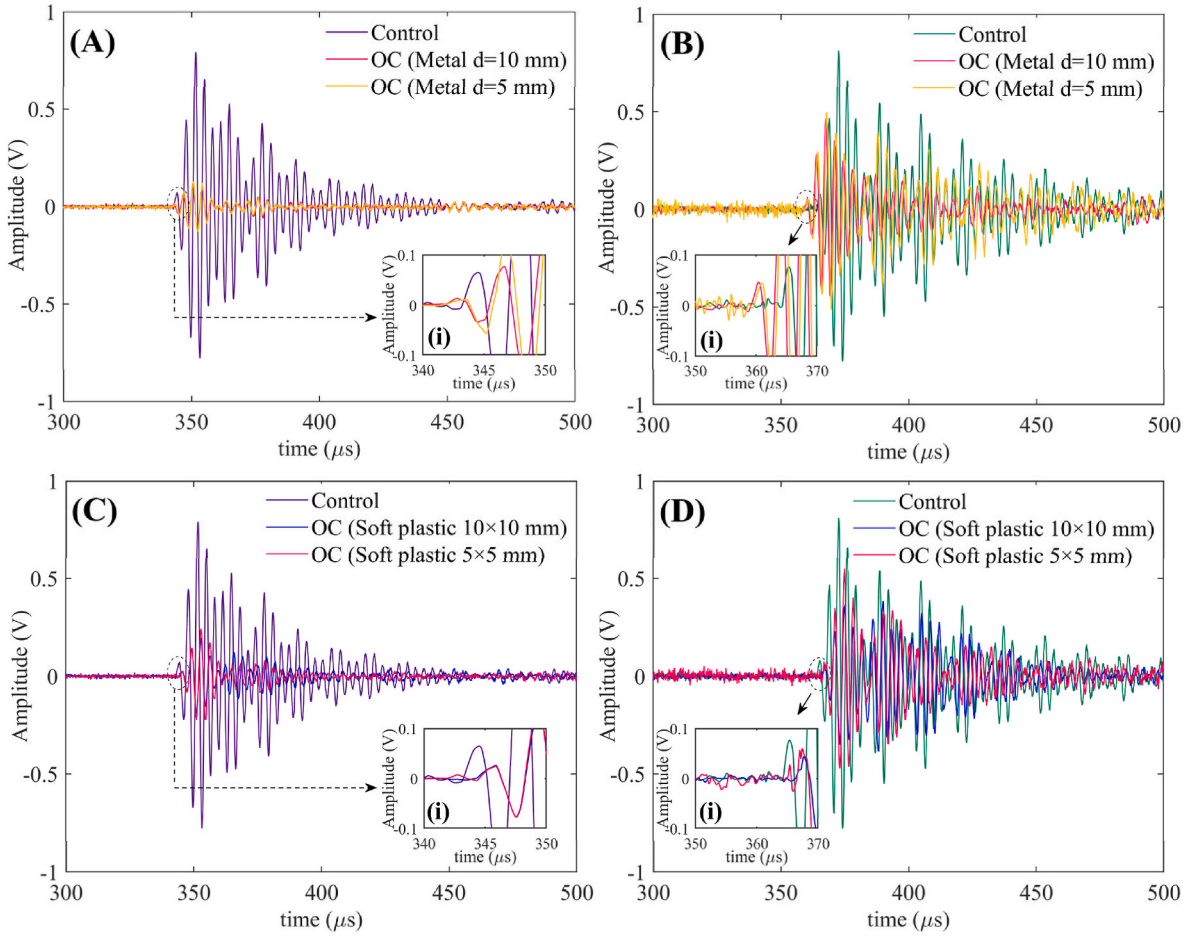

Fig. 3. Ultrasonic signals from the center of Control burger patties (A, C) and jellies (B, D) and with foreign bodies (OC: Out of Control). In the case of samples within foreign bodies, the ultrasonic signals were obtained from the central point in where the greatest effect body was observed. (i) provides a zoomed view of the arrival section of the normalized ultrasonic wave (normalization was done to effectively compare arrival times by adjusting values to a common scale). One of the three signal replicates was randomly selected for display in this figure, as a similar behavior was observed across all replicates.

patties and jellies alter the ultrasound signals. In every case, the FB presence caused a noticeable decrease in the signal amplitude. The FB represents a barrier for the propagation of the ultrasonic wave causing different effects related to wave amplitude reduction. Firstly, the decrease in the A_s is linked to the impedance mismatch between food samples and FBs, which results in a partial reflection of the ultrasonic wave at the food FB interface (Pallav et al., 2009; Fariñas et al., 2021b). In this regard, a higher A_s reduction was observed in the presence of metal (Fig. 3A and B) than plastic pieces (Fig. 3C and D) what can be attributed to the larger impedance mismatch with the food product (Z: metal 22.61 ± 0.09 MRayl, plastic 1.05 ± 0.02 MRayl, burger patties 1.73 ± 0.05 MRayl and jellies 1.37 ± 0.04 MRayl; Table 1). Secondly, the FB may also contribute to additional energy absorption when it exhibits a different attenuation coefficient than the food material. Finally, the presence of the FB may also result in air voids around it, increasing the overall heterogeneity, which largely contributes to the attenuation through scattering (Fariñas et al., 2021b). Among the different phenomena involved in the energy reduction, scattering may play a key role.

In this regard, A_s reduction by FB was larger in burger patties (Fig. 3A and C) compared to jellies (Fig. 3 B and D). This is likely because the FB is fully embedded in the jellies, as it is located in the water-gelatin solution before it solidifies. Thereby, the gel surrounds the FB, minimizing the amount of air trapped between the food and the FB. In contrast, in burgers, the FB is inserted into the solid matrix causing a larger discontinuity (trapped air) between both materials (Fariñas et al., 2021b). Therefore, both the impedance mismatch and the sample placement, potentially involving air trapped around the FB, contribute to the energy loss caused by the FB. These factors may account for the observed reduction in ultrasonic signal amplitude, being less pronounced in jelly plates than in burger patties, as well as for the lesser signal distortion caused by plastic compared to metal.

The presence of FBs also affected the TOF, as illustrated in Fig. 3. A slight leftward shift in the signal was observed in both burger patties (Fig. 3Ai), and jellies (Fig. 3Bi) containing metal FBs, compared to the Control samples. Conversely, a slight delay (rightward shift) in the signal occurred with plastic bodies in both burger patties (Fig. 3Ci) and jellies (Fig. 3Di). These trends can be explained by the distinct properties of the food samples and FBs (Table 1). In this regard, metal (3155.25 ± 15.18 m/s) exhibited a higher v than burger patties (1507.50 ± 25.66 m/s) and jellies (1329.83 ± 27.10 m/s). Conversely, the v in the plastic (917.55 ± 16.42 m/s) was lower than the one found in the food products (Table 1), which explains the delay in the signals recorded with the presence of the plastic FBs (Fig. 3Ci and 3Di). The v calculation is largely dependent on product thickness (Fariñas et al., 2023). This dependency can lead to greater inaccuracies in the calculation of v for products with reduced thickness, such as burgers and jellies. Consequently, industrial testing methods based on v requires precise sample thickness

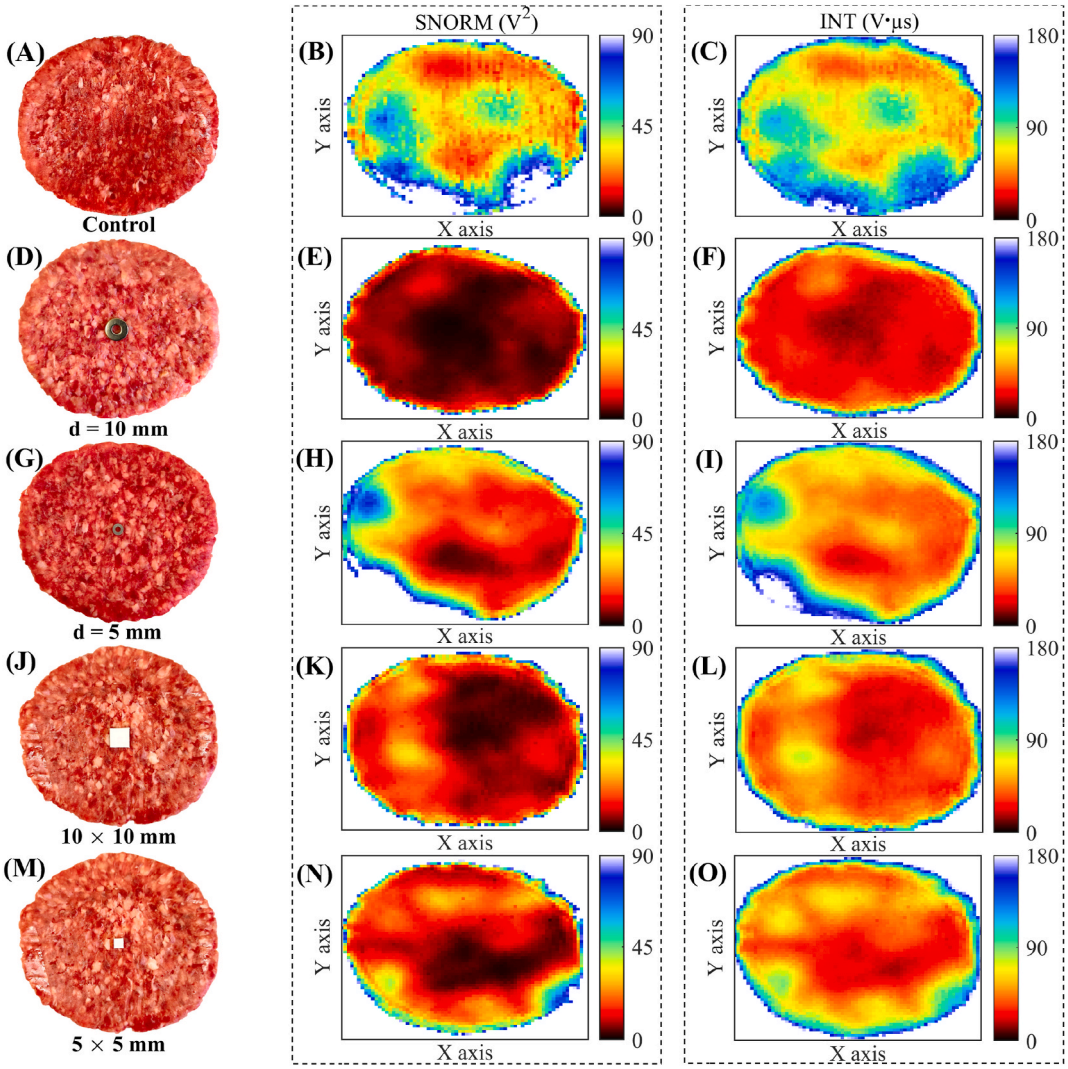

Fig. 4. Air-coupled ultrasound images (80 × 80 mm) of beef burger patties. RGB, SNORM (square norm), and INT (integral) images. One of the three image replicates was randomly selected for display in this figure, as a similar behavior was observed across all replicates.

measurement, which can be challenging for products with irregular surfaces. Therefore, this study will only focus on the use of energy-related parameters for the detection of FBs, as these may be more suitable for industrial applications.

To quantify the energy attenuation caused by the FB, the pixels obtained from the center of Control and OC images of SNORM and INT (Figs. 4 and 5) were analyzed via multifactor ANOVA model (section 2.4, Table 2). Statistically significant differences ($p < 0.05$) were observed in SNORM and INT depending on the food sample, FB type and size. Among the control food samples, jellies exhibited significantly higher SNORM and INT values (69.6 ± 0.2 V^2 and 117.9 ± 0.1 V μs, respectively) compared to burger patties (25.4 ± 0.2 V^2 and 63.2 ± 0.1 V μs, respectively), which is linked to the higher attenuation (scattering effects) in burger patties, caused by their heterogeneity (comprising mixed and conformed lean meat and fat tissues) in contrast to the inherent homogeneity of jellies.

As for the effect of the presence and type of FB, SNORM and INT were noticeably reduced by the FB presence (Table 2). The percentages of reduction for the burger patties were as follows.

- Metal (d = 10 mm): 94.9 % SNORM and 78.3 % INT
- Metal (d = 5 mm): 83.1 % SNORM and 69.1 % INT
- Plastic (10 × 10 mm): 89.4 % SNORM and 71.5 % of INT

Table 2
Influence of foreign bodies on the energy-related ultrasound parameters.

Food samples	Foreign bodies	Size (mm)	SNORM (V^2)	INT (V·μs)
Burger patties	No-presence	–	25.4 ± 0.2^{aA}	63.2 ± 0.1^{aA}
	Metal	10	1.3 ± 0.1^{bA}	13.7 ± 0.1^{bA}
		5	4.3 ± 0.1^{cA}	19.5 ± 0.2^{cA}
	Soft plastic	10 × 10	2.7 ± 0.1^{dA}	18.0 ± 0.1^{dA}
		5 × 5	4.5 ± 0.2^{cA}	20.1 ± 0.1^{eA}
Jellies	No-presence	–	69.6 ± 0.2^{aB}	117.9 ± 0.1^{aB}
	Metal	10	15.9 ± 0.2^{bB}	49.0 ± 0.2^{bB}
		5	19.8 ± 0.1^{cB}	59.3 ± 0.1^{cB}
	Soft plastic	10 × 10	21.6 ± 0.2^{dB}	62.4 ± 0.3^{dB}
		5 × 5	26.9 ± 0.1^{eB}	69.6 ± 0.2^{eB}

SNORM (square norm) and INT (integral). Mean ± standard error of 27 pixels (9 pixels for each image and three replicates) obtained from the center (3 × 3 mm) of SNORM and INT for Control and Out-of-Control samples. Different lowercase and uppercase letters indicate statistically significant differences (95 %) for each energy-related ultrasound parameter with lowercase letters representing differences by foreign body type and uppercase letters representing differences by food material.

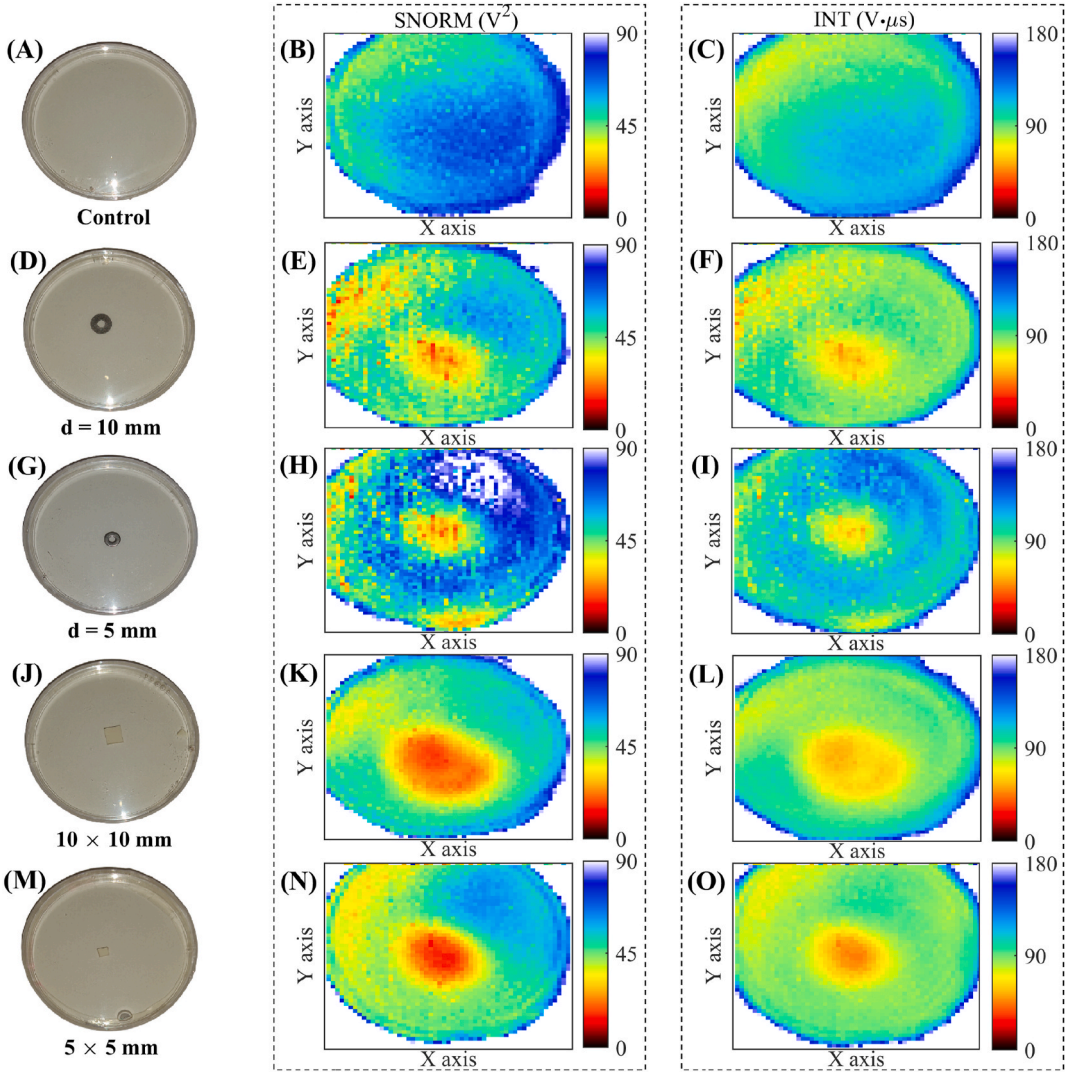

Fig. 5. Air-coupled ultrasound images (60 × 60 mm) of jellies. RGB, SNORM (square norm), and INT (integral) images. One of the three image replicates was randomly selected for display in this figure, as a similar behavior was observed across all replicates.

- Plastic (5 × 5 mm): 82.3 % SNORM and 68.2 % INT

While for the jellies, the reduction percentages were.

- Metal (d = 10 mm): 77.2 % SNORM and 58.4 % INT
- Metal (d = 5 mm): 71.6 % SNORM and 49.7 % INT
- Plastic (10 × 10 mm): 69.0 % SNORM and 47.1 % INT
- Plastic (5 × 5 mm): 61.4 % SNORM and 41.0 % INT

Additionally, based on the results of the multifactor ANOVA models, a detection threshold for FB was established. Pixels in images with SNORM values lower than the thresholds established from the Control food samples (69.6 ± 0.2 V^2 for jellies and 25.4 ± 0.2 V^2 for burger patties) could be attributed to the presence of FB. Conversely, pixels with values equal to or above these thresholds would correspond to the Control food samples. Considering these limits, 100 % of the samples could be correctly classified as OC and 100 % correctly classified as OC using the SNORM parameter. Moreover, a threshold was also established based on the INT parameter, achieving the correct classification of 100 % of both Control and OC samples.

These results demonstrate the feasibility of using air-coupled ultrasound technology for detecting FBs within heterogeneous (e.g., burger patties) and homogeneous (e.g., jellies) food matrices.

Previous studies using contact and air-coupled ultrasound systems have consistently demonstrated that the presence of FBs induces noticeable alterations in ultrasonic wave patterns, specifically an energy drop with the presence of FBs, compared to control signals (Hæggström and Luukkala, 2001; Leemans and Destain, 2009; Meftah and Azimin, 2012; Zhao et al., 2003, 2004, 2006).

3.2. Detection of foreign bodies using air-coupled ultrasound images

Air-coupled ultrasound images (C-scans) of burger patties and jellies are shown in Figs. 4 and 5, respectively, for both Control (Fig. 4A for burgers and Fig. 5A for jellies) and OC samples (Figs. 4–5D, 4-5G, 4–5J and 4–5M). For illustrative purposes, the images shown (Figs. 4 and 5) were randomly selected from the three replicates obtained (section 2.1). A similar behavior was observed in the remaining Control and OC signals. Within the boundaries of burger patties, most of the pixels in the Control ultrasound images of SNORM (Fig. 4B) and INT (Fig. 4C) exhibited pixels values ranging from 19 to 55 V^2 and 45–91 V μs, respectively. These values reflect the inherent variability in the ultrasonic measurements of the Control burger patties, which is attributed to the product's aforementioned heterogeneity.

Despite the inherent natural variability in air-coupled ultrasonic images, the presence of FBs in all OC images led to a significant reduction in the pixel values for both SNORM and INT around the FB location. As shown in Fig. 4, the OC samples with metal (d = 10 mm; 1.3–24 V^2 and 13.7–70 V μs, Fig. 4E and F) and plastic (10 × 10 mm; 2.7–29 V^2 and 18–71 V μs, Fig. 4K and L) exhibited noticeable lower pixel values for both SNORM and INT, compared to Control samples. This energy reduction is manifested in the image as dark red areas, which show an anomalous pattern linked to the location of the FB (Fig. 4). As expected, the color differences (indicating energy decrease compared to control) for OC samples with 5 mm FBs (metal 4.3–55 V^2 and 19.5–90 V μs, Fig. 4H and I and plastic 4.5–55 V^2 and 20.1–85 V μs, Fig. 4N and O) were lower compared to 10 mm FBs size. These findings demonstrate the feasibility of ultrasound imaging for detecting the presence or absence of FBs of different sizes within a burger patty. Areas with pixel values abnormally lower than the ones found in Control samples reveal the presence of FBs. Moreover, the extent of these areas was related to the size of FBs, increasing as the FB size increases, as observed in Figs. 4 and 5. It is important to note that, in all cases, the location of the FB appeared distorted and blurred in the ultrasonic images. This phenomenon, as discussed in section 2.4, occurred because the active area of the ultrasound transducers was much larger than the size of the FB. As a consequence, the affected area, in terms of ultrasonic propagation, extended beyond the FB boundaries. The use of focused transducers could improve the differentiation of the FB and reduce the detection limit for FB size. However, focused transducers would require a larger number of measuring points to cover the entire surface of the scanned samples. Therefore, determining the minimum number of scans is essential and should be addressed in future work, as it plays a critical role, particularly in the industrial implementation of this technology. A preliminary evaluation of the in-line application of air-coupled ultrasound detection of FB using unfocused transducers is presented in Section 3.3.

In the case of jellies (Fig. 5) the variability within the Control images was less pronounced compared to that observed in burger patties due to its more homogeneous nature. Pixel values within the Control jellies images ranged from 45 to 70 V^2 for SNORM and 85–119 V μs for INT. As in the burger patties, the FBs presence was detectable in the ultrasonic images for both SNORM and INT parameters (Fig. 5), for both metal of d = 10 mm (15.9–66 V^2 and 49–95 V μs, Fig. 5E and F) and d = 5 mm (19.8–75 V^2 and 59.3–120 V μs, Fig. 5H and I) and plastic FBs of 10 × 10 mm (21.6–70 V^2 and 62.4–115 V μs, Fig. 5K and L) and 5 × 5 mm (26.9–70 V^2 and 69.6–120 V μs, Fig. 5N and O). When comparing Figs. 4 and 5, it is evident that the FB location is more clearly defined in jellies than in the case of the burger patties. This can be attributed to the more homogeneous nature of jellies compared to the heterogeneous structure of burger patties. Greater heterogeneity in the burger patties leads to increased scattering of the ultrasonic waves, which significantly contributes to the blurring effect observed in the ultrasonic images.

To perform image analysis for defect detection, histograms results are of particular interest as they can identify anomalous pixel distributions (Ezenarro et al., 2023). As an example, Fig. 6 illustrates the INT image histograms and their corresponding cumulative histograms for both Control burger patties (Fig. 4C) and jelly plates (Fig. 5C), as well as those containing plastic with dimensions of 10 × 10 mm (Figs. 4L and 5L, respectively). The histograms for burger patties (Fig. 6A and C) and jellies (Fig. 6B and D) reveal a clear distinction between Control samples and those containing plastic FBs, where the presence of FBs induced a left-skewed distribution and increased tailing. Additionally, the pixel cumulative histograms effectively differentiate control samples from those containing FBs for both burger patties (Fig. 6C) and jellies (Fig. 6D), as indicated by higher frequencies at low INT values found in the pixel cumulative histograms of samples containing FBs.

To quantify the influence of FBs in both the image histograms and cumulative histograms, and to establish a threshold for differentiating the Control and OC samples, the statistical results of multifactor ANOVA model performed on SKE computed from image histograms and the AUC values obtained from the cumulative histograms of both SNORM and INT are presented in Table 3. Statistical analysis revealed significant differences ($p < 0.05$) in SKW and AUC for SNORM and INT image-based histogram analysis. The ANOVA results indicate that the presence of FBs significantly left-skewed the histogram distribution in air-coupled ultrasound images. Larger metal bodies were the most likely to modify the pixel distribution compared to plastic pieces. Additionally, the AUC of cumulative histograms were higher for samples containing FBs than for control samples. This result can be attributed to the energy-attenuation caused by FBs, which concentrates pixels towards lower SNORM and INT values (leftward shift), thereby increasing their frequency and altering the pixel distribution. This effect was less pronounced in the jellies, where the FBs are better embedded within the gel matrix compared to burgers, reducing the distortion of the ultrasonic images, as discussed in section 3.1.

Based on the ANOVA model results, a detection threshold for FB was established. Samples which exhibited AUC values computed from SNORM cumulative histograms exceeding 51.65 ± 0.815 V^2 for burgers and 29.49 ± 1.24 V^2 for jellies were classified as OC (Table 4). Considering these thresholds, 100 % of the samples were correctly classified as Control or OC, using the AUC parameter calculated from

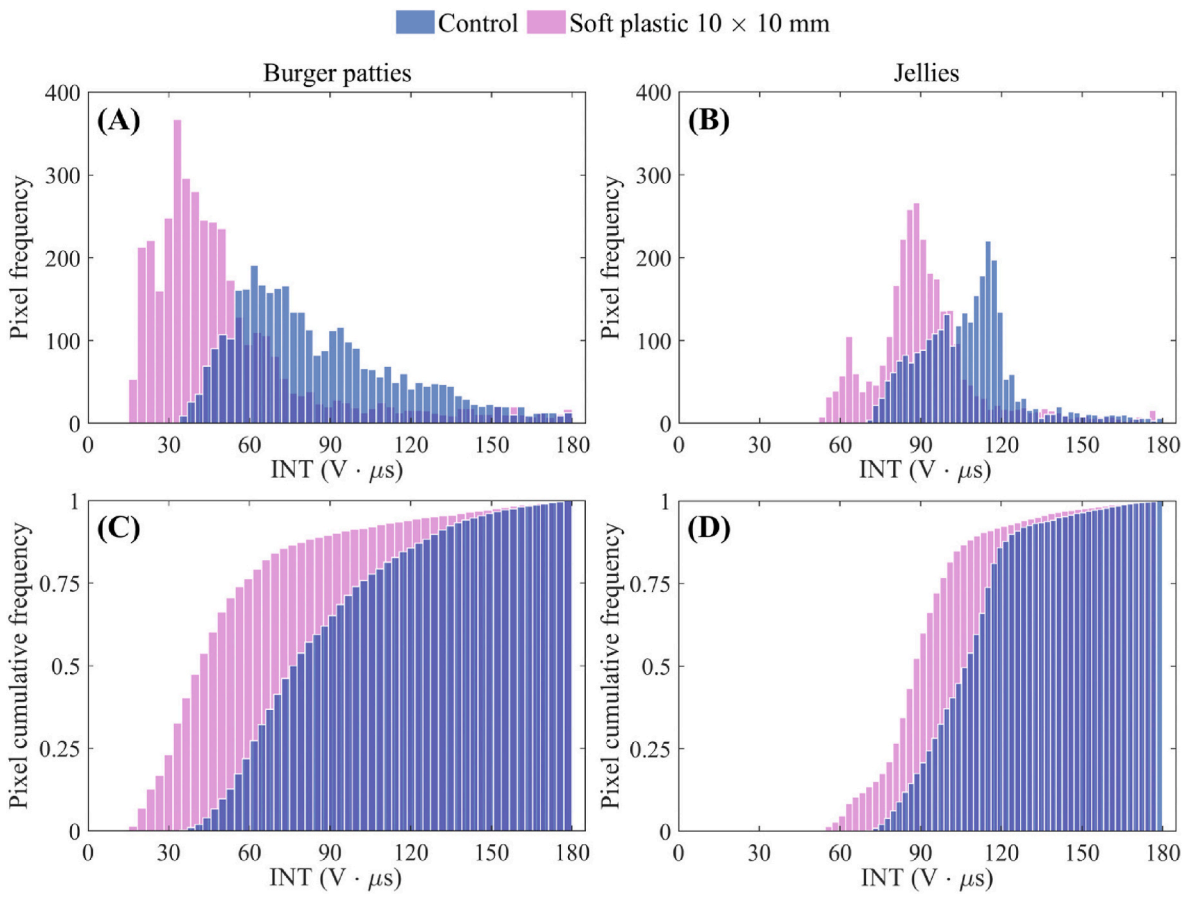

Fig. 6. Image histogram (A, B) and cumulative histogram (C, D) for Control and Out-of-Control (soft plastic 10 × 10 mm) burger patties (A, C) and jellies (B, D). One of the three histogram replicates was randomly selected for display in this figure, as a similar behavior was observed across all replicates.

Table 3
Influence of foreign bodies on the skewness (SKW) and area-under-curve (AUC) computed from histogram analysis of energy-related ultrasound images.

Food samples	Foreign bodies	Size (mm)	Histogram		Cumulative histogram	
			SKW_{SNORM}	SKW_{INT}	AUC_{SNORM} (V^2)	AUC_{INT} (V·μs)
Burger patties	No-presence	–	0.98 ± 0.07^{aA}	0.91 ± 0.05^{aA}	51.65 ± 0.81^{aA}	100.74 ± 1.25^{aA}
	Metal	10	3.38 ± 0.03^{bA}	2.25 ± 0.01^{bA}	80.15 ± 1.21^{bA}	139.50 ± 0.52^{bA}
		5	1.40 ± 0.06^{cA}	1.23 ± 0.02^{cA}	63.74 ± 0.89^{cA}	110.88 ± 0.86^{cA}
	Soft plastic	10 × 10	2.64 ± 0.07^{dA}	1.96 ± 0.03^{dA}	74.72 ± 0.73^{dA}	128.94 ± 0.85^{dA}
		5 × 5	1.95 ± 0.09^{eA}	1.56 ± 0.04^{eA}	71.03 ± 1.01^{eA}	122.55 ± 0.71^{eA}
Jellies	No-presence	–	0.11 ± 0.04^{aB}	0.95 ± 0.06^{aA}	29.49 ± 1.24^{aB}	73.41 ± 2.43^{aB}
	Metal	10	0.42 ± 0.08^{bB}	2.04 ± 0.02^{bB}	41.95 ± 1.48^{bB}	93.87 ± 5.14^{bB}
		5	-0.08 ± 0.03^{cB}	0.51 ± 0.03^{cB}	34.74 ± 0.39^{cB}	81.69 ± 1.93^{cB}
	Soft plastic	10 × 10	0.23 ± 0.07^{dB}	1.41 ± 0.04^{dB}	43.55 ± 1.46^{bB}	91.77 ± 5.61^{bB}
		5 × 5	-0.02 ± 0.03^{cB}	1.95 ± 0.04^{eB}	43.84 ± 1.50^{bB}	94.81 ± 4.92^{bB}

SKW_{SNORM} (skewness of square norm histogram images), SKW_{INT} (skewness of integral histogram images), AUC_{SNORM} (area-under-curve of the cumulative histogram of square norm images) and AUC_{INT} (area-under-curve of the cumulative histogram of integral images). Mean ± standard error. Different lowercase and uppercase letters indicate statistically significant differences (95 %) for each energy-related ultrasound parameter with lowercase letters representing differences by foreign body type and uppercase letters representing differences by food material.

SNORM cumulative histograms. Furthermore, from the thresholds identified for SKE in SNORM and INT histograms and for AUC in INT cumulative histograms, a 100 % correct classification for both Control and OC samples was achieved. Despite the limited sample size, the thresholds defined for both parameters demonstrated the discriminative capability of our system and its reliably distinguishing between samples with and without FBs.

To compare the robustness of the air-coupled ultrasound system presented in this study for potential industrial implementation in the detection of FBs, the SNR values of the ultrasound signals are depicted in Table 4. Additionally, the SNR values of contact and air-coupled ultrasound systems found in literature for food characterization and detection of FBs are also included in Table 4. Previous studies have explored the feasibility of using air-coupled ultrasound imaging to detect FBs in various food matrices. For instance, Pallav et al. (2009) employed a pair of capacitive transducers to acquire ultrasound images, using A_s to detect the presence of wood (10 mm), rubber (2 mm), and glass (2 mm) pieces within cheddar cheese, as well as hazelnuts (5 mm) and mint (3 mm) in chocolate-based products. However, due to the low SNR of the obtained signals (5.7, Table 4), advanced image processing was necessary to enhance image quality and address the challenge of distinguishing between FB-containing areas and the natural background

Table 4
Characterization of signal-to-noise ratio (SNR) of Control and Out-of-Control (OC) air-coupled ultrasound signals and those reported in literature for different contact and air-coupled ultrasound systems.

Air-coupled ultrasound signals			
Food samples	Foreign bodies	Size (mm)	SNR
Burger patties	No-presence	–	56.61
	Metal	10	8.56
		5	16.36
	Soft plastic	10 × 10	11.87
		5 × 5	14.25
Jellies	No-presence	–	25.30
	Metal	10	6.81
		5	13.77
	Soft plastic	10 × 10	9.03
		5 × 5	12.94

Literature reports					
Food sample	**Ultrasound technology**	**Foreign bodies**	**Size (mm)**	**SNR**	**Authors**
Salty margarine	Contact	i) Plastic	10 × 10 × 1	1.63	Hæggström and Luukkala (2001)
		ii) Stones	20 × 10 × 5	2.13	
Canned orange juice	Contact	No-presence	–	2.5	Zhao et al. (2003)
Cheese	Contact	i) No-presence	–	33.7	Leemans and Destain (2009)
		ii) Plastic	Ø = 3	4.35	
Chicken breast	Air-coupled	No-presence	–	8	Cho and Irudayaraj (2003)
Cheese	Air-coupled	No-presence	–	5.70	Pallav et al. (2009)
Beverage can	Air-coupled	No-presence	–	2.5	Ho et al. (2007)
Canned full-fat milk Canned strawberry milk	Air-coupled	No-presence	–	10 9	Gan et al. (2006)

variability in images of FB-free areas. Additionally, Cho & Irudayaraj (2003) used a pair of piezoelectric transducers operating in through-transmission mode at 1 MHz to detect metal rods, metal fragments, and glass fragments of different sizes embedded in cheese and poultry breast, based on amplitude images. This study highlighted the need to compensate for air instability during ultrasound signal acquisition, as the high frequency (1 MHz) piezoelectric transducers used had low stability. This limitation entails important limitations for real industrial application. Ho et al. (2007) used electromagnetic acoustic transducers for canned food products since the measurement requires electrically conductive containers. The SNR of their time-domain signal was 2.5 (Table 4), which is considerably lower than the SNR achieved in our study, ranging from 25.30 to 56.61 for Control and 6.81 to 14.25 for OC (Table 4). Overall, previous studies (Table 4) report significantly lower SNR values (1.63–33.7) than those achieved in the present work (6.81–56.61), which hinders the accurate estimation of ultrasonic parameters and the industrial application. In contrast, the present study demonstrates that unprocessed ultrasonic images differentiate areas with FBs of various types (metal and plastic) in both burgers and jellies, strongly supporting the potential of this technique for industrial implementation. This remarkable detection capability is attributed to the high SNR achieved by the equipment used, particularly due to the custom-built unfocused piezoelectric transducers specifically designed for air-coupled applications.

3.3. Exploring potential industrial application

To explore the implementation of a reliable and robust system for future industrial applications, a possible experimental setup for ultrasound-based FB detection (Fig. 2) is illustrated in Fig. 7. In this configuration, an ultrasound module (Fig. 7A–D) would be integrated between two adjacent belt conveyors (Fig. 7F) designed to transport the product (Fig. 7E) in continuous manufacturing processes. The air-coupled ultrasound sensors are positioned in the gap between these two belt conveyors, allowing the wave to pass unobstructed through the product and reach the receiver transducer. The effective transducers' area must cover most of the product's surface, thus, an array of air-coupled ultrasound sensors (Fig. 7G) may be used to scan the entire food surface, as illustrated in Fig. 7 with a 3-element array. The linear transducer configuration (Fig. 7) is one feasible option, though alternative spatial configurations could also be implemented. Furthermore, while increasing the number of transducer elements in the array can improve coverage, it is essential to balance this with potential effects on measurement accuracy, cost, and equipment complexity.

The ultrasonic images obtained for both Control and OC samples served for simulating the aforementioned industrial application using the configuration described in Fig. 7. Thus, from the ultrasound images of SNORM and INT, three different B-scans were extracted (CSC, LSC and RSC; Fig. 7G). These scans simulate data that would be obtained with the 3-transducer configuration illustrated in Fig. 7, aligning with the expected scan points generated by the conveyor belt movement in an inline system. Specifically, CSC was captured from the center of the images, while LSC and RSC were captured by shifting 15 mm left and right, respectively. The simulated inline B-scans, representing practical

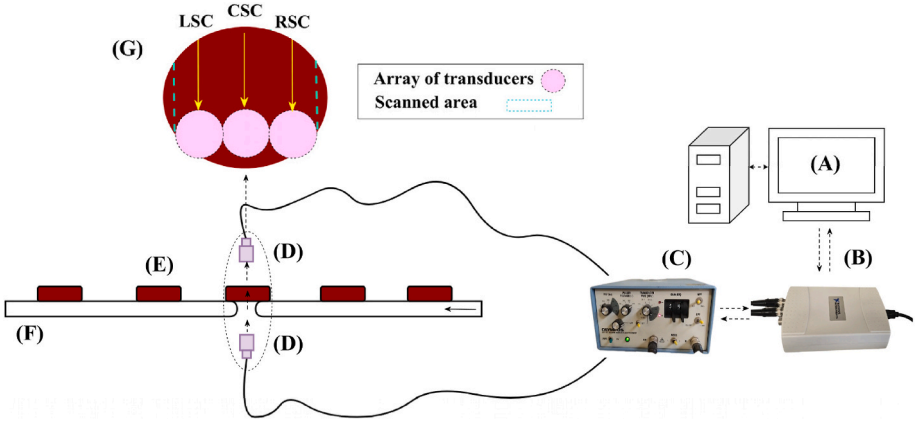

Fig. 7. Possible configuration of an air-coupled ultrasound system for inline detection of foreign bodies. Computer (A), digitizing card (B), pulser-receiver (C), piezoelectric air-coupled ultrasound transducers (D), food sample (E), conveyor belts (F) and scanned area by the transducer array (G): LSC (left scan), CSC (center scan) and RSC (right scan).

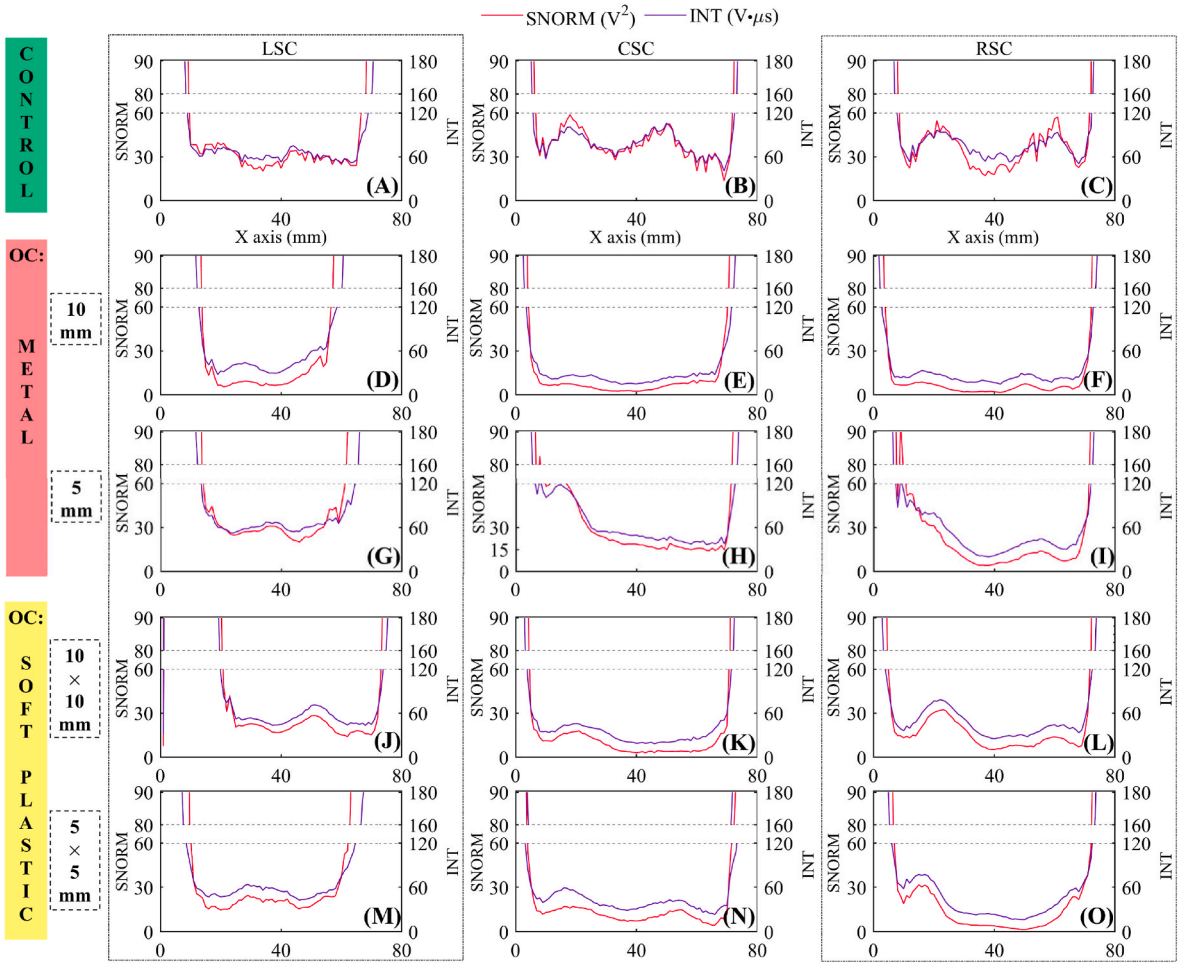

Fig. 8. Inline detection of foreign bodies in burger patties for different transmitter-receiver positions. OC (Out of Control), LSC (left scan), CSC (central scan) and RSC (right scan): SNORM (square norm) and INT (integral). One of the three scan replicates was randomly selected for display in this figure, as a similar behavior was observed across all replicates.

outputs for real-time detection, are shown in Fig. 8 for burger patties and Fig. 9 for jellies. As is illustrated by the left (LSC, Figs. 8A and 9A), center (CSC, Figs. 8B and 9B), and right (RSC, Figs. 8C and 9C) C-scans, a consistent pattern is shown in the Control samples. At the initial (left) and final (right) sections of the SNORM and INT X-scans, the edge effect, or "dead-zone" of the transducer, is observed. This effect arises from the mismatch between the food material and the active area of the transducer, causing a portion of the ultrasonic energy to propagate through the air and alter the energy-related measurements. Consequently, SNORM and INT values are elevated at the product boundaries (dead-zone) and decrease as the alignment between the transducer's active area and the scanned portion of the food improves. The presence of this dead-zone may hinder the detection of FBs located near these boundaries, and addressing its impact will be important in future studies. However, this limitation falls outside the scope of the present work, as FBs were positioned centrally within the food samples to provide an initial evaluation of the feasibility of using unfocused air-coupled transducers for FB detection. One potential strategy to mitigate detection challenges in boundary regions involves covering the outermost boundary with a material that dampens ultrasound signal saturation when the emitter and receiver are aligned and the food surface does not fully cover the transducer's effective area. Another straightforward yet effective strategy is applying a gate to the received signal in order to discard the airborne component. This strategy is feasible in burger and jellies since the ultrasonic velocity is much higher than in the air. While this may result in some loss of relevant data, it effectively mitigates edge effects.

Outside the dead-zone, energy-related parameters remained relatively constant for Control samples. For example, in the CSC of burger patties (Fig. 8A), SNORM values ranged from 19 to 55 V^2, and INT values from 59 to 100 V μs. A similar pattern was observed for jellies, where in the CSC (Fig. 9A) SNORM and INT ranged from 46 to 66 V^2 and from 70 to 108 V μs, respectively.

The effect of the FB is evident when comparing, for example, Fig. 8B and E. The minimum value of Control scan was 19 V^2 for SNORM and 59 V μs for INT. In contrast, the scan with metal of d = 10 mm exhibited minimum values of 2.6 V^2 for SNORM and of 15.4 V μs for INT. As FB size decrease (metal at d = 5 mm), the difference between Control and OC scans became less pronounced. In Fig. 8H, the minimum values of SNORM and INT were of 14.8 V^2 and 42.9 V μs, respectively. The detection efficiency for plastics was similar to that for metals. For the 10 × 10 mm plastic (Fig. 8K), the minimum values of SNORM and INT were 3.1 V^2 and 18.3 V μs, respectively, while for the 5 × 5 mm plastic FB (Fig. 8N), values were 7.2 V^2 for SNORM and 30.7 V μs for INT. In jelly samples, FB location was more easily identified due to sharp changes in the scans, as illustrated in Fig. 9E, H, 9K and 9N.

For the burger patties, the presence of the FB is also evident in some of the RSC (Fig. 8F, I, 8L and 8O), whereas LSC closely resemble those of the control samples. This effect in the RSC scans is primarily attributed to the significant distortion caused by the FB within the ultrasonic image in burger patties and the occasional misalignment of the FB with the patty center during reshaping. The impact of these factors is of less

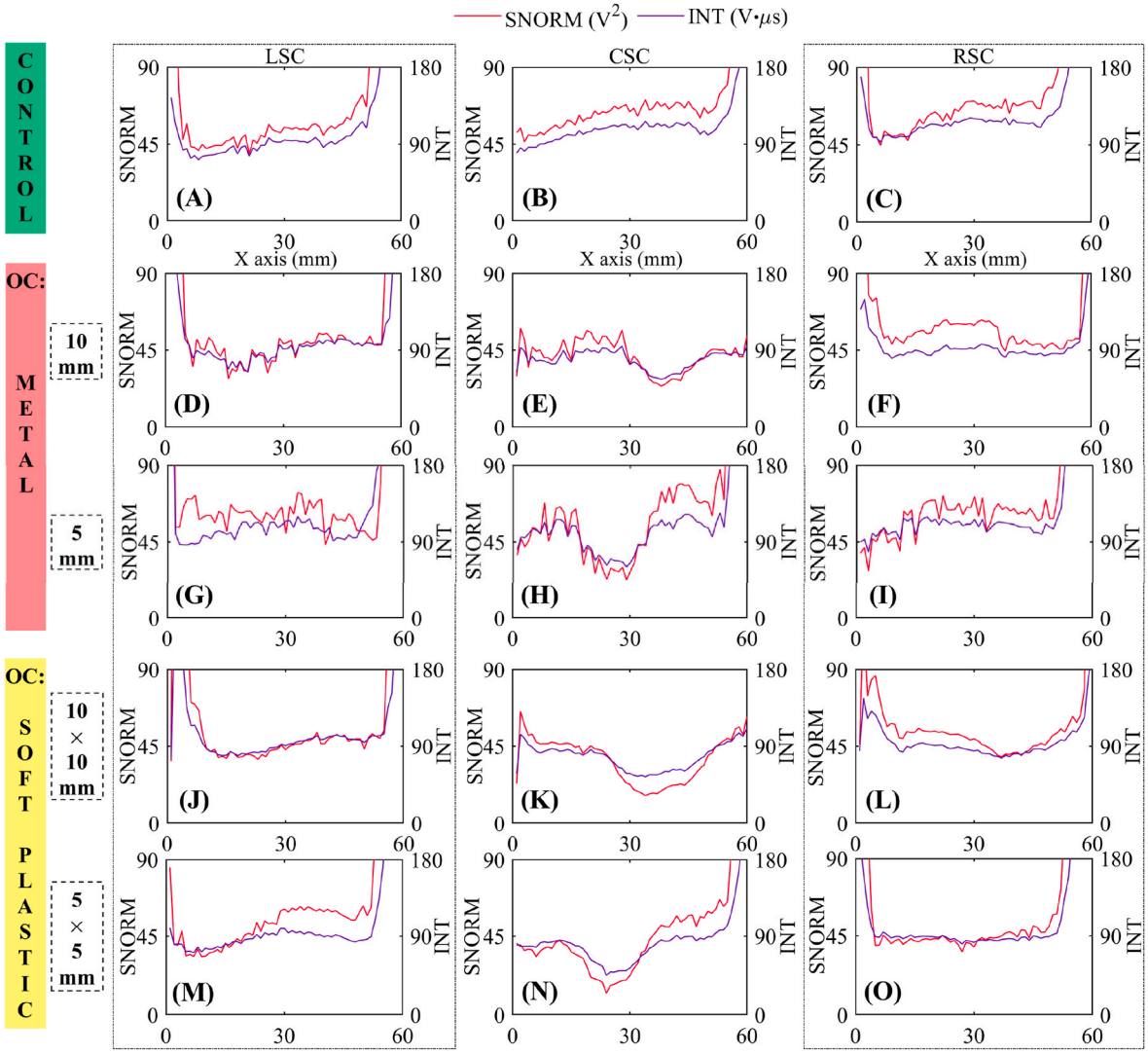

Fig. 9. Inline detection of foreign bodies in jelly plates for different transmitter-receiver positions. OC (Out of Control), LSC (left scan), CSC (central scan) and RSC (right scan): SNORM (square norm) and INT (integral). One of the three scan replicates was randomly selected for display in this figure, as a similar behavior was observed across all replicates.

extent in the jelly plates, thus, RSC and LSC show patterns comparable to the Control scans.

To enhance this analysis, a multifactor ANOVA was conducted to quantify the influence of FB size and type and the food sample type on the area-under-curve of the square norm center scan ($AUC_{SNORM\text{-}CSC}$) and area-under-curve of the integral center scan ($AUC_{INT\text{-}CSC}$) (Table 5). Statistical significant differences ($p < 0.05$) were observed for both $AUC_{SNORM\text{-}CSC}$ and $AUC_{INT\text{-}CSC}$ as a function of the food and FB type. Control samples of burger patties ($AUC_{SNORM\text{-}CSC} = 1546.12 \pm 19.40$ V^2·mm and $AUC_{INT\text{-}CSC} = 3192.25 \pm 13.98$ V μs·mm) and jellies ($AUC_{SNORM\text{-}CSC} = 2582.56 \pm 26.63$ V^2·mm and $AUC_{INT\text{-}CSC} = 4360.66 \pm 41.11$ V μs·mm) exhibited the highest AUC for SNORM and INT scans. Notably, these AUC values were significantly higher ($p < 0.05$) in jellies than in burger patties, likely due to the greater homogeneity of jellies compared to burger patties. The results confirm that the presence of FBs leads to a significant reduction ($p < 0.05$) in the AUC of scans, consistent with the trends observed in sections 3.1 and 3.2; larger FBs caused greater attenuation (Table 5).

The statistical results from the ANOVA models enabled the determination of detection thresholds from scans. Thereby, scans with $AUC_{SNORM\text{-}CSC}$ values bellow 1546.12 ± 19.40 V^2·mm for burgers patties and 2582.56 ± 26.63 V^2·mm for jellies were classified as defective, while those with values above these thresholds were classified as Control. These thresholds allowed for 100 % accurate classification of the samples as either Control or OC. Additionally, thresholds derived from $AUC_{SNORM\text{-}LSC}$, $AUC_{SNORM\text{-}RSC}$, $AUC_{INT\text{-}CSC}$, $AUC_{INT\text{-}LSC}$ and $AUC_{INT\text{-}RSC}$, also achieved 100 % correct classification of the samples.

The approach of using three specific X-scans of ultrasonic images, covering a substantial portion of the product, effectively demonstrated the feasibility of using unfocused ultrasonic transducers for FB detection in solid and semi-solid foods in industrial applications. This type of transducer allows for broad product coverage while minimizing the number of elements required in the ultrasonic arrays.

This study represents a first step toward developing an accurate and robust system for detecting internal FBs in both unstructured foods (e.g., burger patties) and packaged foods (e.g., jellies) using high-SNR, non-contact ultrasound transducers with excellent air stability. This advancement significantly addresses the challenges of implementing a non-destructive and non-invasive system suitable for food quality monitoring in industrial environments. Future research should examine the detection of FBs located near the edges of food products, as well as establish the detection limits of this technology for small FBs of different materials, such as glass, stones, or biological contaminants, that may be introduced during the manufacturing process. Furthermore, testing a

Table 5
Inline detection of foreign bodies using the area-under-curve (AUC) of the energy-related ultrasound scans positioned in the center of food samples.

Food samples	Foreign bodies	Size (mm)	$AUC_{SNORM\text{-}CSC}$ (V^2·mm)	$AUC_{INT\text{-}CSC}$ (V·μs·mm)
Burger patties	No-presence	–	1546.12 ± 19.40^{aA}	3192.25 ± 13.98^{aA}
	Metal	10	186.70 ± 10.93^{bA}	819.57 ± 29.21^{bA}
		5	837.98 ± 4.39^{cA}	2089.68 ± 19.82^{cA}
	Soft plastic	10 × 10	275.39 ± 10.33^{dA}	1108.99 ± 25.44^{dA}
		5 × 5	419.18 ± 26.21^{eA}	1441.39 ± 64.39^{eA}
Jellies	No-presence	–	2582.56 ± 26.63^{aB}	4360.66 ± 41.11^{aB}
	Metal	10	1644.06 ± 12.31^{bB}	3083.70 ± 8.71^{bB}
		5	2093.37 ± 12.53^{cB}	3808.67 ± 7.16^{cB}
	Soft plastic	10 × 10	1289.03 ± 33.98^{dB}	2855.76 ± 44.17^{dB}
		5 × 5	1471.85 ± 25.52^{eB}	2916.78 ± 21.49^{dB}

$AUC_{SNORM\text{-}CSC}$ (area-under-curve of the square norm center scan) and $AUC_{INT\text{-}CSC}$ (area-under-curve of the integral center scan). Mean ± standard error. Different lowercase and uppercase letters indicate statistically significant differences (95 %) for each energy-related ultrasound parameter with lowercase letters representing differences by foreign body type and uppercase letters representing differences by food material.

larger sample set is essential to developing a robust statistical framework that supports real-time FB detection and comprehensive quality monitoring across the entire food production process.

4. Conclusions

The presence of foreign bodies in food samples caused alterations in the transmitted ultrasound waves, leading to a decrease in energy-related ultrasound parameters. The interaction between the ultrasonic wave and the foreign body results in energy loss, which depends heavily on the foreign body's material, size, and the properties of the surrounding food matrix. Metal pieces produced greater attenuation in the air-coupled ultrasound signals compared to plastic pieces. Additionally, larger foreign bodies caused a more significant drop in ultrasound signal energy. The impact on ultrasonic parameters was more pronounced in burgers than in jellies, owing to their greater structural heterogeneity.

Acoustic images (C-Scans) generated from energy-related parameters enabled the identification of foreign bodies by comparing pixel patterns with those of the Control samples. From the threshold identified through pixel and histogram image analysis, a satisfactory detection of the presence of foreign bodies embedded within the food samples was achieved, illustrating the potential industrial application of ultrasonic technology.

Air-coupled ultrasound technology could be scaled up for industrial use by employing an array of transducers that cover the entire surface of the product as it moves along a conveyor belt. The use of unfocused transducers minimizes the number of transducers required, thereby reducing costs and system complexity. However, this approach lowers spatial resolution, complicates FB size determination, and is susceptible to the edge effect caused by airborne wave interference. Depending on the specific requirements of each application, different solutions may be more suitable, balancing resolution, cost, and robustness against edge effects. Future studies should investigate detection limits based on the nature of the foreign body and the specific configuration of the ultrasonic array, including factors like geometry, number of elements, and operating frequency. The full development of air-coupled ultrasound technology has the potential to enable real-time monitoring across the entire food production process.

CRediT authorship contribution statement

Gentil A. Collazos-Escobar: Software, Investigation, Formal analysis, Data curation. **José M. Prats-Montalbán:** Writing – review & editing, Software, Methodology, Funding acquisition, Data curation, Conceptualization. **Anabella S. Giacomozzi:** Writing – review & editing, Investigation, Formal analysis. **José Benedito:** Writing – review & editing, Supervision, Project administration, Funding acquisition, Formal analysis, Conceptualization. **Tomas E. Gómez Álvarez-Arenas:** Writing – review & editing, Methodology, Formal analysis, Conceptualization. **José V. García-Pérez:** Writing – review & editing, Supervision, Methodology, Investigation, Funding acquisition, Formal analysis, Conceptualization.

Declaration of competing interest

None.

Acknowledgments

The authors express their gratitude for the funding provided by the ULTRADIGITAL project (AGROALNEXT/2022/045) as part of the AGROALNEXT program. This program is supported by the MCIN, with funding from the European Union NextGenerationEU (PRTR-C17.I1), as well as the Generalitat Valenciana. Additionally, Gentil A. Collazos-Escobar's doctoral scholarship (PRE2020-092255) is acknowledged, which was granted through the State Training Subprogram of the State Plan for Scientific and Technical Research and Innovation 2017–2020, in conjunction with the European Social Fund.

Data availability

Data will be made available on request.

References

Álvarez-Arenas, G.E.T., 2004. Acoustic impedance matching of piezoelectric transducers to the air. IEEE Trans. Ultrason. Ferroelectrics Freq. Control 51, 624–633. https://doi.org/10.1109/TUFFC.2004.1320834.

Awad, T.S., Moharram, H.A., Shaltout, O.E., Asker, D., Youssef, M.M., 2012. Applications of ultrasound in analysis, processing and quality control of food: a review. Food Res. Int. 48 (2), 410–427. https://doi.org/10.1016/j.foodres.2012.05.004.

Chandrapala, J., 2015. Low intensity ultrasound applications on food systems. Int. Food Res. J. 22 (Issue 3).

Chen, Q., Zhang, C., Zhao, J., Ouyang, Q., 2013. Recent advances in emerging imaging techniques for non-destructive detection of food quality and safety. TrAC, Trends Anal. Chem. 52, 261–274. https://doi.org/10.1016/j.trac.2013.09.007. Elsevier B.V.

Chimenti, D.E., 2014. Review of air-coupled ultrasonic materials characterization. Ultrasonics 54 (7), 1804–1816. https://doi.org/10.1016/j.ultras.2014.02.006.

Cho, B.K., Irudayaraj, J.M.K., 2003. Foreign object and internal disorder detection in food materials using noncontact ultrasound imaging. J. Food Sci. 68 (3), 967–974. https://doi.org/10.1111/j.1365-2621.2003.tb08272.x.

Collazos-Escobar, G.A., Gutiérrez-Guzmán, N., Váquiro-Herrera, H.A., Bon, J., Cárcel, J. A., García-Pérez, J.V., 2023. Model-based investigation of water adsorption in Achira (Canna edulis K.) biscuits. LWT 189. https://doi.org/10.1016/j.lwt.2023.115472.

Djekic, I., Jankovic, D., Rajkovic, A., 2017. Analysis of foreign bodies present in European food using data from Rapid Alert System for Food and Feed (RASFF). Food Control 79, 143–149. https://doi.org/10.1016/j.foodcont.2017.03.047.

Edwards, M.C., Stringer, M.F., 2007. Observations on patterns in foreign material investigations. Food Control 18, 773–782. https://doi.org/10.1016/j.foodcont.2006.01.007.

Ezenarro, J., García-Pizarro, Á., Busto, O., de Juan, A., Boqué, R., 2023. Analysing olive ripening with digital image RGB histograms. Anal. Chim. Acta 1280. https://doi.org/10.1016/j.aca.2023.341884.

Fariñas, L., Contreras, M., Sanchez-Jimenez, V., Benedito, J., Garcia-Perez, J.V., 2021a. Use of air-coupled ultrasound for the non-invasive characterization of the textural properties of pork burger patties. J. Food Eng. 297. https://doi.org/10.1016/j.jfoodeng.2021.110481. December 2020.

Fariñas, L., Sanchez-Torres, E.A., Sanchez-Jimenez, V., Diaz, R., Benedito, J., Garcia-Perez, J.V., 2021b. Assessment of avocado textural changes during ripening by using contactless air-coupled ultrasound. J. Food Eng. 289. https://doi.org/10.1016/j.jfoodeng.2020.110266. July 2020.

Fariñas, M.D., Sanchez-Jimenez, V., Benedito, J., Garcia-Perez, J.V., 2023. Monitoring physicochemical modifications in beef steaks during dry salting using contact and

non-contact ultrasonic techniques. Meat Sci. 204, 109275. https://doi.org/10.1016/j.meatsci.2023.109275.

Gan, T.H., Pallav, P., Hutchins, D.A., 2006. Non-contact ultrasonic quality measurements of food products. J. Food Eng. 77 (2), 239–247. https://doi.org/10.1016/j.jfoodeng.2005.06.026.

Garcia-Perez, J.V., de Prados, M., Martinez, G., Gomez Alvarez-Arenas, T.E., Benedito, J., 2019. Ultrasonic online monitoring of the ham salting process. Methods for signal analysis: time of flight calculation. J. Food Eng. 263, 87–95. https://doi.org/10.1016/j.jfoodeng.2019.05.032. May.

Hæggström, E., Luukkala, M., 2001. Ultrasound detection and identification of foreign bodies in food products. Food Control 12 (1), 37–45. https://doi.org/10.1016/S0956-7135(00)00007-4.

Ho, K.S., Billson, D.R., Hutchins, D.A., 2007. Inspection of drinks cans using non-contact electromagnetic acoustic transducers. J. Food Eng. 80 (2), 431–444. https://doi.org/10.1016/j.jfoodeng.2006.04.025.

Leemans, V., Destain, M.F., 2009. Ultrasonic internal defect detection in cheese. J. Food Eng. 90 (3), 333–340. https://doi.org/10.1016/j.jfoodeng.2008.06.042.

Li, F., Liu, Z., Sun, T., Ma, Y., Ding, X., 2015. Confocal three-dimensional micro X-ray scatter imaging for non-destructive detecting foreign bodies with low density and low-Z materials in food products. Food Control 54, 120–125. https://doi.org/10.1016/j.foodcont.2015.01.043.

Meftah, Azimin, M., 2012. Detection of foreign bodies in canned foods using ultrasonic testing. Int. Food Res. J. 19 (2).

Mohd Khairi, M.T., Ibrahim, S., Md Yunus, M.A., Faramarzi, M., 2015. Contact and non-contact ultrasonic measurement in the food industry: a review. Meas. Sci. Technol. 27 (1). https://doi.org/10.1088/0957-0233/27/1/012001.

Mohd Khairi, M.T., Ibrahim, S., Md Yunus, M.A., Faramarzi, M., 2018. Noninvasive techniques for detection of foreign bodies in food: a review. J. Food Process. Eng. 41 (6). https://doi.org/10.1111/jfpe.12808. Blackwell Publishing Inc.

Pallav, P., Hutchins, D.A., Gan, T.H., 2009. Air-coupled ultrasonic evaluation of food materials. Ultrasonics 49 (2), 244–253. https://doi.org/10.1016/j.ultras.2008.09.002.

Sanchez-Jimenez, V., Collazos-Escobar, G.A., González-Mohino, A., Gomez Alvarez-Arenas, T.E., Benedito, J., Garcia-Perez, J.V., 2023. Non-invasive monitoring of potato drying by means of air-coupled ultrasound. Food Control 148. https://doi.org/10.1016/j.foodcont.2023.109653.

Yaqoob, M., Sharma, S., Aggarwal, P., 2021. Imaging techniques in Agro-industry and their applications, a review. J. Food Meas. Char. 15 (3), 2329–2343. https://doi.org/10.1007/s11694-021-00809-w. Springer.

Zhao, B., Basir, O.A., Mittal, G.S., 2003. Detection of metal, glass and plastic pieces in bottled beverages using ultrasound. Food Res. Int. 36 (5), 513–521. https://doi.org/10.1016/S0963-9969(02)00201-6.

Zhao, B., Jiang, Y., Basir, O.A., Mittal, G.S., 2004. Foreign body detection in foods using the ultrasound pulse/echo method. J. Food Qual. 27 (4), 274–288. https://doi.org/10.1111/j.1745-4557.2004.00651.x.

Zhao, B., Yang, P., Basir, O.A., Mittal, G.S., 2006. Ultrasound based glass fragments detection in glass containers filled with beverages using neural networks and short time Fourier transform. Food Res. Int. 39 (6), 686–695. https://doi.org/10.1016/j.foodres.2006.01.008.